# Quantitative ultrasound techniques for assessing thermal ablation: Measurement of the backscatter coefficient from ex vivo human liver

Adrien Rohfritsch, Emilie Franceschini, Aurélien Dupré, David Melodelima

# Quantitative ultrasound techniques for assessing thermal ablation: Measurement of the backscatter coefficient from ex vivo human liver

Adrien Rohfritsch,[1*] Emilie Franceschini,[2] Aurélien Dupré[1], David Melodelima[1]

[1]LabTAU, INSERM, Centre Léon Bérard, Université Lyon 1, Univ Lyon, F-69003, LYON, France

[2]Aix-Marseille Université, CNRS, Centrale Marseille, LMA, Marseille, France

Version typeset September 22, 2023

Author to whom correspondence should be addressed. email: adrien.rohfritsch@inserm.fr

**Abstract**

**Background:** Understanding the changes occurring in biological tissue during thermal ablation is at the heart of many current challenges in both therapy and medical imaging research.
**Purpose:** The objective of this work is to quantitatively interpret the scattering response of human liver samples, before and after thermal ablation. We report acoustic measurements performed involving n = 21 human liver samples. Thermal ablation is achieved at temperatures between 45°C and 80°C and quantification of the irreversible changes in acoustic attenuation and Backscattering Coefficient is reported, with a particular attention to the latter.
**Methods:** Both attenuation coefficient and Backscattering Coefficients were measured in the frequency range from 10 to 52 MHz. Scans were performed before heating and after cooling down. Attenuation coefficients were calculated using spectral difference method and Backscattering coefficient estimated using the reference phantom method.
**Results:** Strong increases of attenuation coefficients and Backscattering Coefficients with heating temperature were observed. Quantitative ultrasonic parameters obtained with the polydisperse structure factor model are compared to histological observations and seen to be close to hepatocyte mean diameter.
**Conclusions:** The results presented in this study provide a description of the impact of thermal ablation in human liver tissue on acoustic attenuation and the BSC. For the first time, quantitative agreement between the Effective Scatterer Diameter estimated from Backscattering Coefficient and hepatocyte mean diameter was shown, highlighting the important role of cellular network in the scattering response of the medium. This core result is an important step toward the determination of the nature of scattering sources in biological tissues.

# I. Introduction

# Introduction

Determining the nature of scatterers is essential not only for current ultrasound imaging methods but also for the use of these techniques in new applications such as thermal monitoring. During thermal ablation, many phenomena are likely to change scattering sources, such as tissue expansion, cell death and coagulation. During heating, thermal and structural changes jointly appear and are intrinsically linked. Together, they induce an increase of the backscattered ultrasonic energy that can be imaged using ultrasound[1,2,3]. However, precise physical origins of this phenomenon have never been described in biological tissue, preventing the use of these imaging modalities to monitor tissue ablation. An important barrier that prevents such understanding is the question of the dominant source of scattering in biological tissues. This question has already been discussed recently[4,5,6] and is at the heart of our study.

Quantitative Ultrasound (QUS) techniques provide insight into tissue microstructure and are based on the frequency analysis of the backscattered signals. To date, they have been used in many medical contexts, such as bone structural characterization[7], diagnosis of liver steatosis[8,9,10] or monitoring of High Intensity Focused Ultrasound (HIFU) treatment[5]. Different parameters have been adopted as QUS parameters. Some have been obtained by linear regression of the tissue power spectrum[11], and others have been determined based on fine interpretation of the backscattering response of heterogeneous media based on the Backscattering Coefficient (BSC). The latter requires analytical models that express the BSC with the help of structural characteristics[12] such as the Effective Scatterers Diameter (ESD). Different models exist, the most widely used being the Spherical Gaussian Model (SGM) and the Fluid Sphere Model (FSM). If these models are based on different descriptions of disorder (continuous impedance variation for the SGM; a random distribution of discrete scatterers for the FSM), they both rely on the assumption of a diluted and perfectly disordered medium. However, these assumptions become incorrect in the case of a dense medium, where spatial correlation appears due to positional constraints between scatterers close to each other. To overcome this issue, a polydisperse Structure Factor Model (poly-SFM) was proposed to investigate backscattering from correlated media comprising an ensemble of polydisperse spheres or aggregates[13]. This model was used as a framework to determine what are scatterers in normal and heated human liver tissues. To experimentally assess the BSC of liver tissue, attenu-

ation effects must be compensated between the region of interest and the surface of the imaging probe. As reported by Suomi *et al.*, the attenuation of various liver samples is on average twice as high after thermal ablation[14]. Therefore, careful estimation of the attenuation during and after thermal exposure is mandatory to precisely estimate QUS parameters based on the BSC.

The objective of the present work is to characterize ultrasound scattering sources in the human liver at different temperatures (from 37°C to 80°C) and to present associated changes in acoustic parameters (attenuation, BSC and QUS parameters).

# II. Methods

## II.A. Human liver samples

Human liver samples were obtained from patients undergoing standard hepatectomy for resectable liver tumors. Twenty-four samples were studied after patients signed informed consent documents. Only a part of the liver resection was used for ultrasonic measurements, the remaining part being used for anatomopathological examination. Anatomopathological analysis revealed that samples from three patients were steatotic (grade $> 0$, the grade being defined with the help of fat inclusion concentration[15,16]). These three patients were excluded from the study, leading to $n = 21$ included samples (one sample per patient). The ultrasonic measurements were performed within two hours after hepatectomy.

## II.B. Ultrasonic data acquisition

Ultrasonic data were acquired using a high-frequency ultrasound system (Vevo 770, Visualsonics Inc, Toronto, ON, Canada). Two probes, RMV 710 and RMV 704, were used in B-mode. Regarding the RMV 710 and the RMV 704 probes, the oscillating single-element-focused circular transducers had center frequencies of 20 and 40 MHz with 6-dB bandwidths of 8–32 and 30–52 MHz and focus values of 15 and 6 mm (f-numbers of 2.1 and 1.7, respectively). The raw RF data were digitized at a sampling frequency of 250 MHz (8-bit precision) using a high-speed acquisition card (CS11G8, Gage, Lockport, IL, USA). During the experiments, the focus of each transducer was positioned between 0.1 and 0.2 mm below the water/sample interface. Twelve independent B-mode images were constructed from the acquired RF echoes. Regarding BSC estimation, the

images were averaged, and at least five positions were scanned per sample. The signals were gated with a rectangular window with a length of 30 wavelengths at the central frequency in water. The power spectra of the gated RF signals were then averaged to assess $P_{\text{meas}}$.

## II.C. Attenuation

Several methods have been developed to calculate the attenuation of biological tissues[17,18]. Here, we used the spectral difference method, which involves the comparison of two backscattered RF signals acquired with the focal zone at depths $z_1$ and $z_2$ ($\Delta z = z_2 - z_1 > 0$) inside the sample. $P_{\text{meas}}(z_1, f)$ and $P_{\text{meas}}(z_2, f)$ are the power spectra of the RF signals windowed around the focal zone (window width: $30\lambda$, with $\lambda$ the wavelength at central frequency). In this way, the attenuation $\alpha(f)$ (expressed in Np/cm) was calculated as

$$\alpha(f) = \frac{1}{4\Delta z} \ln\left(\frac{P_{\text{meas}}(z_1, f)}{P_{\text{meas}}(z_2, f)}\right), \tag{1}$$

where $f$ is the frequency. The measured attenuation $\alpha(f)$ was then fitted with the power law $\alpha_0 f^b$ to estimate the attenuation coefficient $\alpha_0$ in Np/(cm.MHz$^b$) and the exponent $b$.

## II.D. BSC experimental assessment

The BSC is one of the inherent characteristics of biological tissues, such as attenuation. Depending on the tissue heterogeneity, spatial fluctuations in these parameters can be observed. Here, with the idea of characterizing the global structural changes induced by temperature elevation, global quantities were considered, experimentally measured and averaged over the entire sample. The BSC can be straightforwardly linked to the spectral power density of the backscattered RF signals (see Ultrasonic Data Acquisition). To estimate the BSC, one must compensate for the electromechanical system response and the depth-dependent diffraction and focusing effects caused by the ultrasound beam. To achieve this, the normalization technique used in the present work consists of using a reference phantom, of which the BSC can be determined[19]. This method has been validated to be robust compared with other backscatter coefficient methods, such as the planar reflector method[20]. Considering that the RF signals were windowed around the region of interest at depth $z$ and noting respectively $P_{\text{meas}}$ and $P_{\text{ref}}$ i.e., the power densities inside the sample of interest and inside the reference medium, respectively, the measured BSC, BSC$_{\text{meas}}$, can be expressed as:

$$\mathrm{BSC}_{\mathrm{meas}}(f) = \mathrm{BSC}_{\mathrm{ref}}(f)\frac{P_{\mathrm{meas}}(f)}{P_{\mathrm{ref}}(f)}\frac{e^{4\alpha(f,T)z}}{e^{4\alpha_{\mathrm{ref}}(f)z}}. \quad (2)$$

where $\alpha$ and $\alpha_{\mathrm{ref}}$ are the attenuations of the sample and of the reference medium, respectively, accounting for the losses due to absorption and scattering between the interface of the sample and the region of interest. The reference phantom was provided by the University of Wisconsin (WI, USA) and consisted of 6g/L of glass beads with radii ranging from 0.4 to 6 $\mu$m in a gel-surrounding medium. The reference phantom has been characterized to measure its backscatter coefficient $\mathrm{BSC}_{\mathrm{ref}}$ on the 10-52 MHz frequency bandwidth using a planar reflector and focused transducers having different center frequencies 15, 35 and 55 MHz[21]. Eq. (2) is used to experimentally assess the BSC of the samples.

## II.E. QUS parameters estimation

As briefly mentioned in the Introduction, biological tissues can be considered from a microscopic point of view as a set of fluid scatterers randomly distributed in a homogeneous medium[4]. Shear effects are commonly neglected, so only scattered pressure waves are created throughout the propagation of the incident ultrasonic wave. Under this assumption, the backscattering cross-section of each particle can be described with the help of Anderson's theory[22]. Moreover, multiple scattering effects were neglected (Born approximation) so that the scattering amplitudes of all scatterers were assumed to be independent. Spatial correlation due to the packing effect at the cellular level imposes spatial organization at the same time.

Within this framework, the BSC can be analytically described by the polydisperse structure factor model (poly-SFM)[23,24]. Regarding a dense medium comprising a mixture of spheres differing only in size, with number density $n_0$, the theoretical $\mathrm{BSC} = \mathrm{BSC}_{\text{poly-SFM}}$ is of the form[24,25]:

$$\begin{aligned}\mathrm{BSC}_{\text{poly-SFM}}(k) =& n_0 \int_0^{+\infty} |\Phi(k,r)|^2 p(r)\mathrm{d}r + \\ & n_0 \int_0^{+\infty}\int_0^{+\infty} \Phi(k,r_1)\Phi(k,r_2)H_{12}(k)p(r_1)p(r_2)\mathrm{d}r_1\mathrm{d}r_2, \end{aligned} \quad (3)$$

where $H_{12}$ is the partial structure function, $\Phi$ is the scattering amplitude of the sphere of radius $r$ and $p(r)$ is the sphere radius probability distribution function (i.e., the probability for a sphere to exhibit a radius $r$). The analytical expression of Eq. (3) is given by Griffith et al.[25] and Han and

O'Brien[24] when the scattering amplitude is derived from the fluid-filled sphere form factor given by[24]

$$\Phi(k,r) = \frac{\gamma_z}{4k}\left[\sin(2kr) - 2kr\cos(2kr)\right]. \tag{4}$$

and when the distribution of the sphere radii follows a Gamma (Schulz) probability density function given by

$$p(r) = \frac{1}{\zeta!}\left(\frac{\zeta+1}{a}\right)^{\zeta+1} r^{\zeta} e^{-(\zeta+1)r/a}, \tag{5}$$

where $a$ is the mean radius and $z$ is the gamma width factor ($\zeta > -1$). The gamma width factor measures the width of the gamma distribution (a large value of the gamma width factor $\zeta$ corresponds to a narrow size distribution). It is related to the standard deviation $SD$ of the scatterer diameter as follows: $SD = 2a/\sqrt{\zeta+1}$.

Fitting $\text{BSC}_{\text{meas}}$ with expression (3) allows us to estimate four QUS parameters: the effective scatterers diameter (ESD=2a), the impedance contrast between the host medium and scatterers $\gamma_z = (Z - Z_0)/Z_0$ ($Z$ being the impedance of the scatterers, $Z_0$ is that of the host medium), the spatial concentration $\phi$ and the polydispersity factor $\zeta$ (or equivalently the standard deviation of scatterer diameter SD). Examples of $\text{BSC}_{\text{poly-SFM}}$ evolution with various ESD, $\phi$ and $\zeta$ are reported in Appendix A for various values of these parameters to help the reader understand the link between microstructure properties and BSC behavior.

To estimate these QUS parameters, the experimental average $\text{BSC}_{\text{meas}}$ are fitted to the theoretical BSC given by Eq. (3) using a minimization technique. We defined the metric $F$ to be minimized as

$$F = \sum_j \frac{(\text{BSC}_{\text{poly-SFM}}(k_j) - \text{BSC}_{\text{meas}}(k_j))^2}{\text{BSC}^2_{\text{meas}}(k_j)}. \tag{6}$$

where $k_j = 2\pi f_j/c_0$ is the discrete wavenumber (the frequency step $\Delta f = f_2 - f_1$ being of 131.2kHz). The metric $F$ was chosen among other possibilities in order to weight all frequencies equally and to sum up relative errors[23]. In contrast to Kemmerer *et al.*[26], we performed the optimization process over the whole frequency range accessible with our experimental setup (10-52 MHz), in order to include as much information as possible in the frequency optimization process.

### II.F. Heating/cooling process

All data were acquired in a water bath at a temperature $T = 37$°C. A first set of RF data was acquired in a water bath at a controlled temperature $T > 37$°C. Then, the samples were heated in a second water bath. Five temperatures were chosen: $45$°C ($n = 3$), $55$°C ($n = 4$), $62.5$°C ($n = 4$), $70$°C ($n = 6$) and $80$°C ($n = 4$). The temperature of the water bath was always 1 or 2°C higher than the targeted temperature, and the time needed to heat the samples was approximately 5 minutes for all 21 samples. The sample dimensions varied between 3 and 5 cm$^3$. The temperature evolution of the water and at the center of the sample was monitored with two thermocouple needles (MT-29/5HT, Phymep, Paris, France, diameter 0.33 mm). Once the targeted temperature was reached, the samples were immediately immersed in the first bath at a controlled temperature of $T = 37$°C. After cooling, a second set of RF data was acquired in the same manner as the first one.

## III. Results

### III.A. Attenuation in human liver at different temperatures

For the first time, to our knowledge, the attenuation of the human liver heated at different temperatures is reported within the frequency range from 8 to 52 MHz. These values are crucial to properly estimate the BSC and therefore infer structural changes owing to QUS parameters. For most biological tissues, a close linear behavior of the attenuation is expected, which can be expressed as $\alpha(f) = \alpha_0 f^b$, where the exponent $b$ is usually close to unity. In Figure 1, parameters $\alpha_0$ and $b$ are reported, for all $n = 21$ samples investigated in this study. For each sample an average process was performed over three pairs of images, and each pair was acquired with a focal spot at two depths $z_1$ (ranging between 0.1 and 0.3 mm below the sample interface) and $z_2$, facilitating the estimation of $\alpha(f)$ by means of Eq. (1). Vertical translation was $\Delta z = z_2 - z_1 = 2$ mm for the RMV710 probe and $\Delta z = 1$ mm for the RMV704 probe. Power law fitting was performed with the MATLAB Curve Fitting Toolbox, and no constraints were imposed on parameter $b$.

In Figure 1 (A) and (B), the dots at $T = 37$°C correspond to values before heating. The average value of $\alpha_0 = 0.09 \pm 0.02$ Np/(cm.MHz$^b$) is close to that obtained in prior studies.[27]. Variations were attributed to differences in the fat content.

The higher the heating temperature is, the higher the attenuation after cooling down is. This

highlights the increase in the viscosity of the heated samples and demonstrates that this increase is irreversible; all measurements were performed at $T = 37$°C. As shown in Figure 1 (B), the parameter $b$ remains close to unity in all cases. This allows us to compare one $\alpha_0$ value to the others without interpretation mistakes.

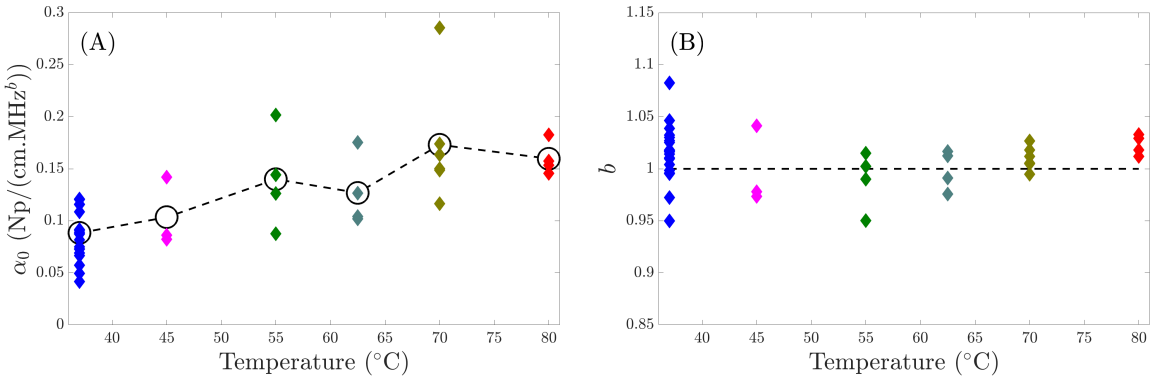


Figure 1: (A) Attenuation coefficient $\alpha_0$ and (B) exponent $b$
, with respect to temperature exposure. The values at $T = 37$°C correspond to the baseline (estimation before heating).

The variability in the attenuation coefficient of unheated samples is a source of possible bias. For this reason, the relative variation of attenuation coefficient at $f = 10$ MHz is shown in Figure 2. In regard to the lowest temperature elevation $T = 45$°C, no increase in attenuation was observed. Therefore, at this temperature, no irreversible changes in the viscosity were observed. At the higher temperature elevations, the relative variations increased. At the highest temperatures $T \geq 70$°C, average attenuation coefficients s were twice stronger than the baseline average value (obtained before heating). Larger variations are observed for $T = 70$°C, which is the sign of a transition occurring around this temperature.

As described in previous studies[26,28], this increase in the viscosity is linked to protein denaturation at temperatures $T \geq 50$°C. This is consistent with the almost unchanged value measured for the lowest temperature ($T = 45$°C), as shown in Figures 1 and 2. The report of attenuation coefficients in heated human liver tissue provides essential information concerning structural changes resulting from microscopic changes at the cellular level. Knowledge of this quantity is required to properly estimate the local scattering response (through the BSC) which is at the core of the next sections.

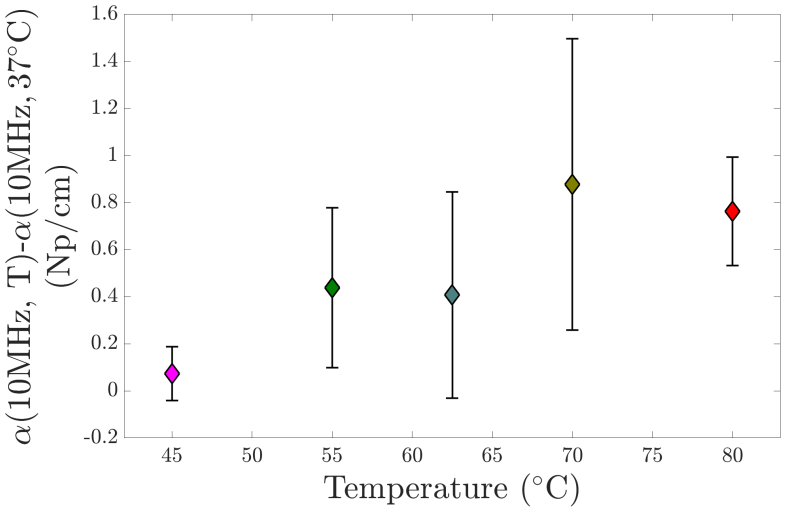


Figure 2: Average values of the difference between the attenuations before and after the heating process at the different temperatures at $f = 10$ MHz.

## Backscattering coefficient and structural change characterization

### BSC variations

Figure 3(A-E) shows of the samples heated at the different temperatures, from $45$°C to $80$°C. All of the samples were compensated for attenuation effects, with the attenuation coefficient of each sample evaluated before and after heating (please refer to the previous section). As this quantity heavily impacts BSC estimation, intervals containing BSC estimates with an attenuation coefficient $\alpha(f) \pm 10\%$ are represented by colored areas around the main curve corresponding to the BSC compensated with attenuation coefficient $\alpha(f)$. Even if the threshold of $10\%$ is arbitrary, much higher than measurements uncertainty, it allows us to quantify the error potentially induced by $\alpha(f)$ misestimation. The impact of this potential error on QUS parameters is discussed in the next sections.

BSC variation evaluation over the largest possible frequency range allows better estimation of the linear relationship of the integrated BSC with the particle concentration in phantoms.[29]. Differences in the integrated BSCs before heating and after cooling are shown in Figure 3(F), for all the samples, revealing that the backscattered energy increased with temperature. The difference between the baseline value ($T = 37$°C, before heating) and the BSC after cooling is four times larger at the heating temperature $T = 80$°C than for $T = 45$°C, for which almost no BSC difference was observed (see Figure 3 (A)). Interestingly, a plateau was reached between 55 and 62.5°C, temper-

atures at which the attenuation coefficient smootly decreases according to the results presented in Figure 1.

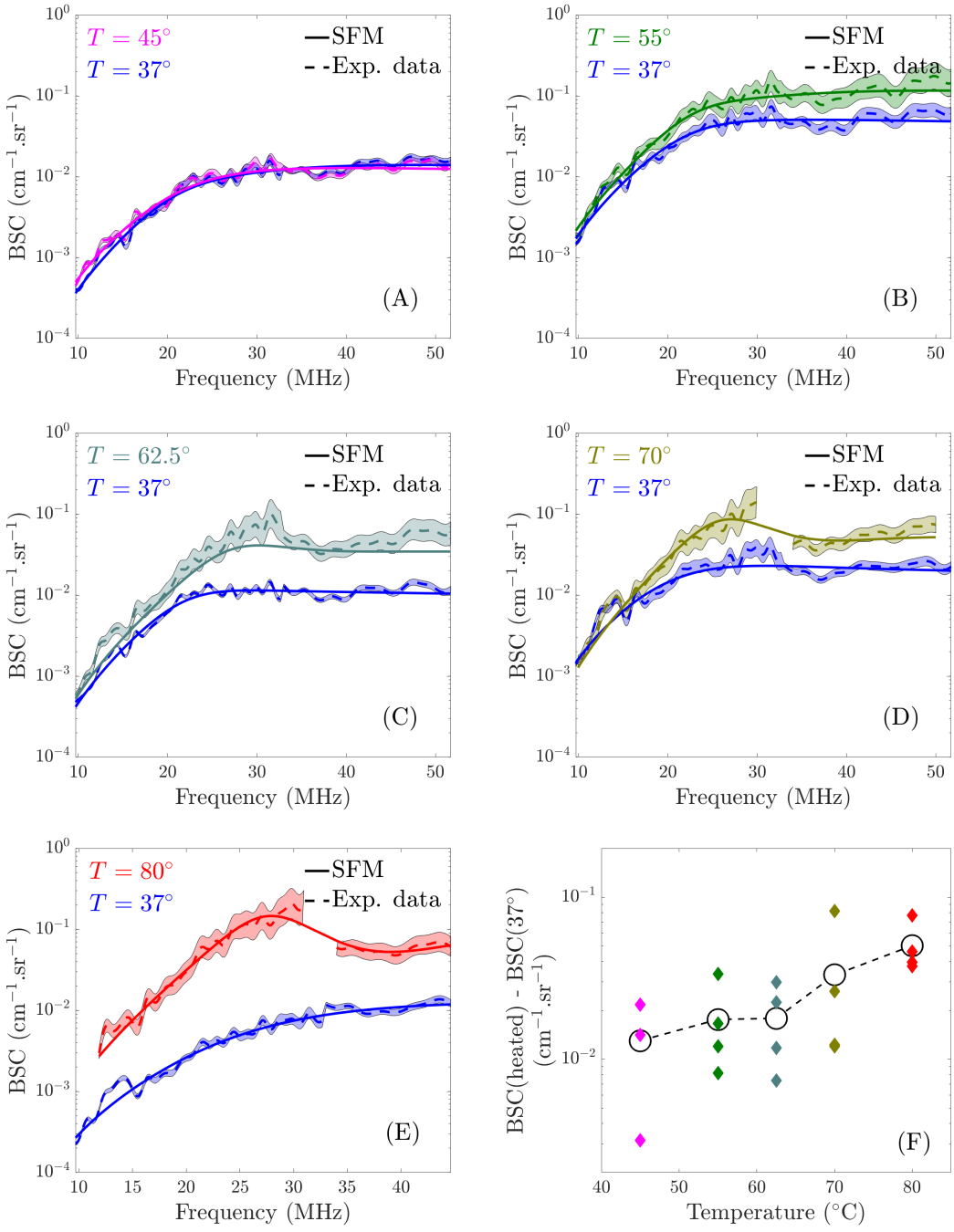


Figure 3: (A)-(E) Examples of BSC measurements for five samples heated at five temperatures. Dotted lines: experimental data; continuous lines: fitted curve obtained by minimization with poly-SFM. The blue lines correspond to unheated tissue. (A) to (E) - 45°C to 80°C. (F) Variations integrated over the whole frequency range, as a function of the temperature for all the $n = 21$ samples.

# IV. Comparison to histological sections

Facing the difficulty of determining the nature of scattering sources inside biological tissues, the comparison of ESD values predicted by poly-SFM to histological observations is of paramount interest. This allows us to build a bridge between ultrasonic measures and structural changes in such tissues. This comparison is only possible because thermal effects were eliminated during BSC measurement.

Five samples were selected and stained with the red Sirius method[30], which is often used in collagen detection. Two groups of histological sections were obtained for each sample: the first one before heating and the second one after cooling. In this manner, each sample was used as its own reference and heated at a given temperature (45, 55, 62.5, 70 and 80°C).

Hepatocytes were detected in each histological section. Hepatocytes have a polygonal shape, and the mean diameter was derived from their area $S$ such as HMD $= 2\sqrt{\frac{S}{\pi}}$. Four examples are shown in Figure 4, with the corresponding HMD distributions. These four sections correspond to two samples heated at $T = 45$°C (A-D) and at $T = 70$°C (E-H). It should be noted that the radii and polydispersity factor values extracted through the analysis of 2D histological sections do not faithfully mimic the 3D medium[31].

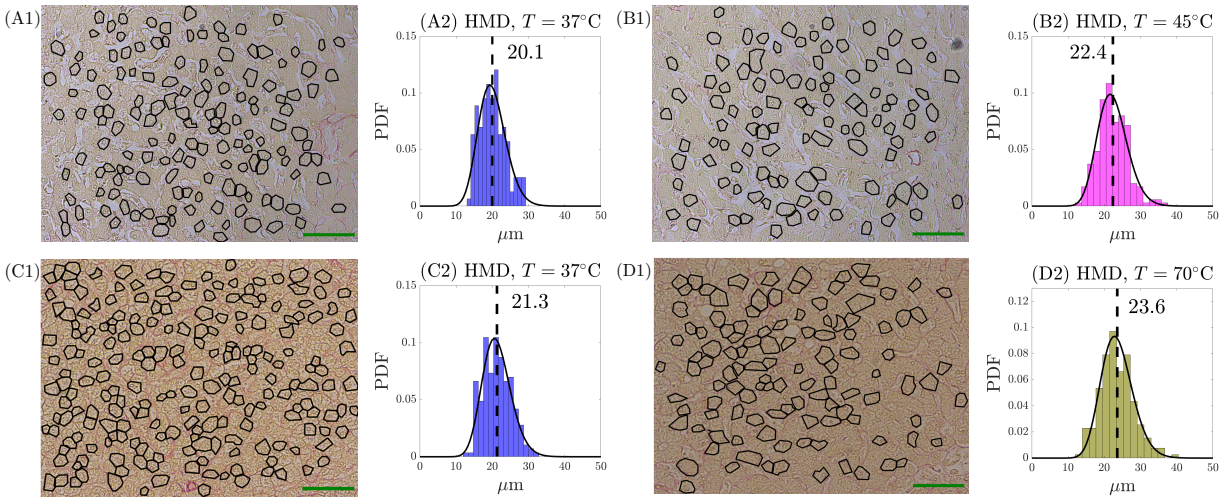


Figure 4: (A1), (B1), (C1), (D1) : Histological sections (Red Sirius staining method) of four samples. Distributions of HMD, expressed in term of probability densities (PDF), are given in (A2), (B2), (C2), (D2). Top : sample heated at 45°C. Bottom : sample heated at 70°C. PDFs are fitted with the Gamma–Schultz distribution function and vertical dotted lines indicate their respective average HMD value. Scale bar on histological sections is 100 $\mu$m.

As determined in the previous section, poly-SFM depends on four parameters. The multiple

minima that coexist in the 4D space defined by the potential values of the four parameters make the search for solutions challenging. To achieve this, limiting the optimization procedure to a physically acceptable subspace is more relevant than trying to identify the global minimum in the entire 4D space. This strategy is physically acceptable, considering that the parameter values are themselves restricted to specific intervals. Therefore, four intervals were defined, as reported in Table 1. ESD interval was chosen to cover a diameter range that includes both nuclear diameters ($d_{\text{nucl}} = 7.2 \pm 0.39 \mu m$[32]) and cell diameters ($\approx 20\mu$m). These values should avoid any bias in conclusions regarding the origin of scattering events in liver tissue within the frequency range used in our experimental setup. In this wide frequency range, many important scattering contributions may coexist. Therefore, the goal here is not to identify a single scattering source inside the medium but to obtain the order of magnitude for the size of the main contributor to scattering. The interval for the impedance contrast was chosen as $\gamma_z \in [0.01; 0.1]$, which agrees with the approach adopted in previous studies, such as Franceschini *et al.* dealing with K562 cells[33] or Falou *et al.* focused on human acute myeloid leukemia[34]. The width factor $\zeta$ was restricted to the interval $[2; 70]$, which also agrees with that employed in previous works[24,35].

Table 1: Minimum and maximum QUS parameter values delimiting the 4D space where the minimization process is performed to fit experimental BSC values with poly-SFM.

| poly-SFM parameters | min | max |
|---|---|---|
| ESD ($\mu$m) | 0.2 | 40 |
| Concentration | 0 | 1 |
| Impedance contraste $\gamma_z$ | 0.01 | 0.1 |
| Width factor $\zeta$ | 2 | 70 |

Before analyzing the QUS parameters obtained with this optimization procedure, let us briefly present the impact on the estimation of an error of $\pm 10\%$ on $\alpha(f)$. To do so, QUS parameters were estimated with the BSC compensated for attenuation effects with $0.9\alpha(f)$, $\alpha(f)$ and $1.1\alpha(f)$, yielding to three values for each parameter and each sample before and after the heating process. For the sake of legibility, here we only report the ratios of the standard deviation $\sigma$ over the mean value $\mu$ for a given sample and a given QUS parameter. All the ratios are reported in Table 2. Some QUS parameters were highly sensitive to this variability in the attenuation coefficient (i.e., showing a variability greater than $10\%$), highlighting the importance of a suitable precision in $\alpha(f)$ estimation. Nevertheless, almost all the averaged variations were smaller than $10\%$, except

for $\zeta$. Specifically, the ESD and $\phi$ were less sensitive to the attenuation variations than $\zeta$ and $\gamma_z$. In the figures and discussions that follow, the QUS parameters obtained from BSCs compensated for attenuation with $\alpha(f)$ will be shown.

Table 2: Standard deviation $\sigma$ devided by average value $\mu$ of all QUS parameters estimated with poly-SFM from the experimental BSC measurements before and after heating, when compensation for attenuation effects is performed with attenuation coefficients $0.9\alpha(f), \alpha(f)$ and $1.1\alpha(f)$ (please refer to the text).

| T (°C) | $\frac{\sigma_{\text{ESD}}}{\mu_{\text{ESD}}}$ Unheated/heated (%) | $\frac{\sigma_{\gamma_z}}{\mu_{\gamma_z}}$ Unheated/heated (%) | $\frac{\sigma_{\phi}}{\mu_{\phi}}$ Unheated/heated (%) | $\frac{\sigma_{\zeta}}{\mu_{\zeta}}$ Unheated/heated (%) |
|---|---|---|---|---|
| 37 / 45 | 2.2 / 2.3 | 3.2 / 3.4 | 2.4 / 2.8 | 7.8 / 12 |
| 37 / 55 | 10.4 / 0.60 | 9.6 / 8.3 | 18 / 2.0 | 89 / 5.8 |
| 37 / 63 | 1.4 / 1.9 | 3.5 / 13.9 | 1.2 / 1.8 | 4.1 / 31 |
| 37 / 70 | 3.0 / 1.1 | 7.0 / 14.9 | 10 / 0.80 | 31 / 48 |
| 37 / 80 | 15 / 2.1 | 2.2 / 16.3 | 7.9 / 1.6 | 8.1 / 23 |
| **Average** | **6.6 / 1.6** | **4.4 / 11** | **7.9 / 3.1** | **28 / 24** |

All the QUS parameters are shown in Figures 6, 7 and B. Figure 6 shows the estimated ESD $\pm$ the standard deviation and the hepatocyte mean diameter $\pm$ the standard deviation (obtained from the histological sections).

Figure 6(A) shows that the hepatocyte diameters of unheated tissue strongly varied from one sample to another. This variation was quantitatively reproduced by the ESD predictions based on poly-SFM, even if the standard deviations of the ESD values were much larger than those of the hepatocyte mean diameter values (please also refer to Table 3). This variability between the unheated samples was also visible in B-mode images as an increase in echogenicity (Figure 5). This supports the choice of analyzing each sample as its own reference.

Figure 6(B) compares the same quantities as those depicted in (A) for heated tissues. The global conclusions remain unchanged: the order of magnitude of the ESD values is the same as that of the hepatocyte mean diameters (please also refer to Table 3).

Altogether, results presented in Figure 6 lead to the idea that the size of principal scattering sources inside liver tissue is of the same order of magnitude as the HMD. As mentioned previously, nuclear diameter $d_{\text{nucl}}$ is approximately three times smaller than the reported HMD. Therefore, ESD values are always closer to HMD than to $d_{\text{nucl}}$. This is a core result of this paper as it provides new answers on the main scattering sources inside human liver for the frequency range considered (10-52 MHz).

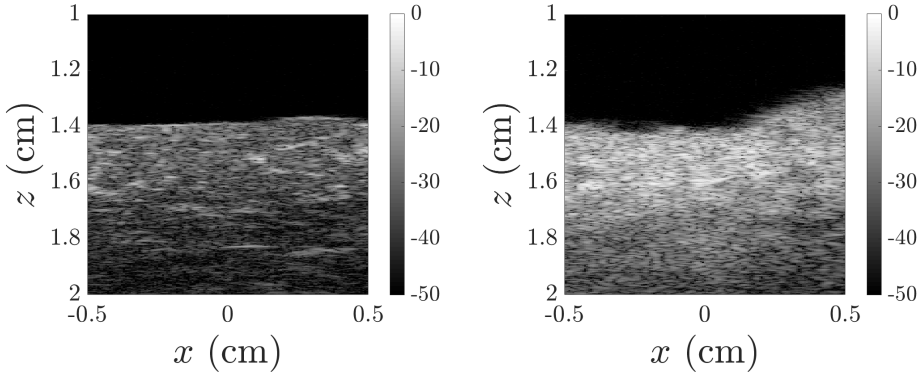


Figure 5: Examples of Bmode images of unheated human liver tissue acquired with the RMV710 probe. The normalization is the same for both images, illustrating strong variations of echogeneicity between the human liver samples.

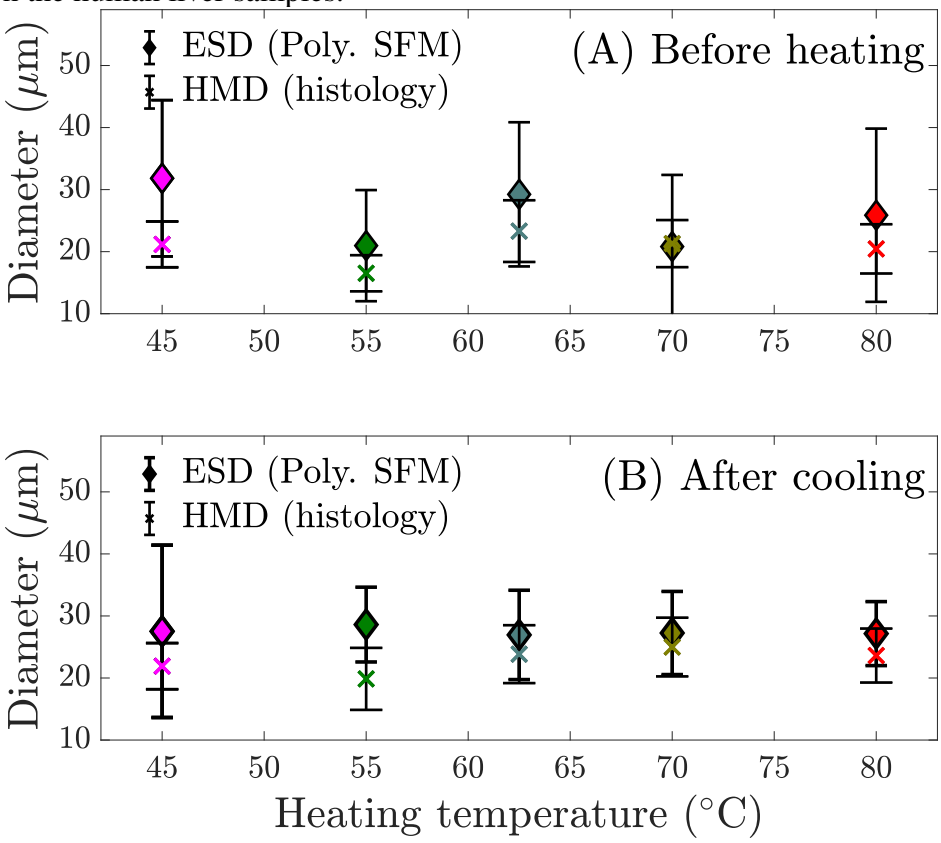


Figure 6: Blue crosses: Mean diameter $\pm$ standard deviation of hepatocytes, measured on histological sections. Red diamonds: ESD $\pm$ standard deviation, estimated by poly-SFM. (A) Before heating process, (B) after cooling.

To expand the analysis, variations of HMD (before and after the heating process) are presented as a function variations of ESD (estimated with poly-SFM) in Figure 7. The variance for each temperature is obtained by adding the variances of diameter distributions before heating ($\sigma^2_{BH}$) and after heating ($\sigma^2_{AH}$). The Person's correlation coefficient is equal to 0.72. The large

Table 3: Hepatocytes mean diameters (HMD) of the different human liver samples heated at the different temperatures, and the corresponding values of scatterer diameter (ESD) and standard deviation (SD) obtained by fitting the BSC experimental results with poly-SFM. The estimated standard deviation of the scatterer diameter is calculated as: SD $=$ ESD$/\sqrt{\zeta+1}$).

| T (°C) | HMD ± SD (histology) | ESD ± SD (poly-SFM) | Relative changes in HMD (histology) | Relative changes in ESD (poly-SFM) |
|---|---|---|---|---|
| 37 / 45 | 20.1±3.6 / 22.6±4.1 | 32.7±12.6 / 28.8±13.9 | 7.0% | -13.8% |
| 37 / 55 | 16.6±2.9 / 19.9±5.0 | 19.9±9.0 / 28.4±6.0 | 20.3% | 43.3% |
| 37 / 62.5 | 23.3±5.0 / 23.8±4.7 | 29.0±11.6 / 26.4±7.2 | 2.3% | -8.9% |
| 37 / 70 | 21.3±3.8 / 25.0±4.7 | 22.1±11.5/ 26.5±5.2 | 17.4% | 22.6% |
| 37 / 80 | 20.4±4.0 / 23.6±4.4 | 27.8±14.0 / 25.8±7.8 | 15.5% | -4.9% |

standard deviations around the ESD variations are due to large polydispersity in both ESD before and after heating.

This prospective result goes beyond the conclusion based on Figure 6: not only are the absolute values of ESD close to HMD, but their variation before and after the heating process are positively correlated. This opening result reveals multiple questions on the number of contributors to scattering and the influence of ablation on their respective weight. These questions will be adressed in future work.

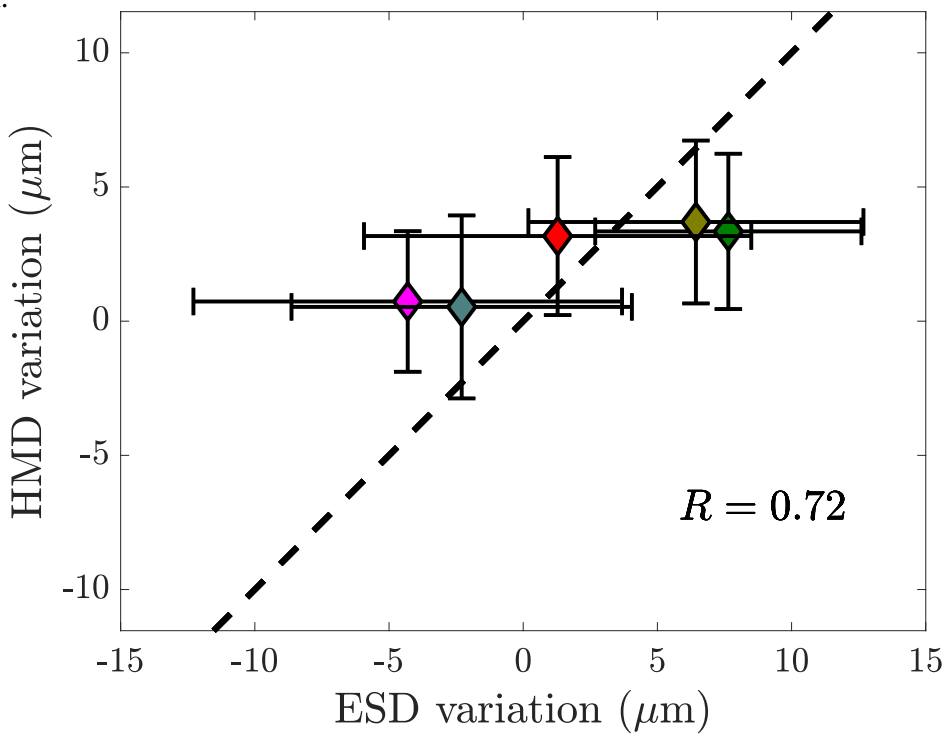


Figure 7: HMD variations before/after heating process as a function of ESD variations, for the five same samples reported in Figure 6 (A) and (B). Dotted line correspond to $y = x$. Pearson coefficient is $R = 0.72$.

The width factor $\zeta$ given by poly-SFM yielded a much larger standard deviation than that

obtained with the hepatocyte diameter distribution. These differences are also reported in Table 3 *via* the standard deviation SD $=$ ESD$/\sqrt{\zeta+1}$ which is a more intuitive parameter than $\zeta$ to grasp size distributions compared to the form factor $\zeta$. This difference may be explained by the fact that other contributors to scattering exist and could comprise cell aggregates with notable size variation. This also agrees with reported values of the ESD that are never smaller than the hepatocyte mean diameter.

Thus, the variation in ESD between a sample heated at 55°C and a sample heated at 62.5°C follows the same decreasing trend as hepatocytes. In contrast, between two saples heated at 62.5°C and 70°C, this trend is increasing. This provides important answers regarding the origin of scattering in human liver tissue and is therefore a core result of this paper.

The QUS parameters $\phi$ (concentration) and $\gamma_z$ (impedance contrast) seem to be impacted by the heating process only for temperature of $T = 80$°C. Moreover, values of these parameters can hardly be compared with histological observations and such comparison is out of the scope of this study. For this reason, all values are reported in Appendix, in Figure B.

Sufficiently high ultrasonic frequencies are required to estimate microstructural parameters at the scale of the nuclei or whole cells. It is well known that a frequency range that satisfies $ka = k\text{ESD}/2 \approx 1$ is recommended for the estimation of QUS parameters[36]. Around this frequency, a resonance marking the size of the principal source of scattering appears. This implies frequencies of around 25 MHz to estimate ESDs around 20 $\mu$m corresponding to the size of whole hepatocytes. It is worth noting that such a resonance is clearly visible in Figure 3 (C-E). This resonance cannot be due to nuclei scattering. However, it is worth noting that a resonance due to nuclei should appear in a frequency range around 65MHz, which is slightly higher than the range considered in this study. A single resonance is visible in all the frequency range, which justifies the choice of performing an optimization process over the whole band, instead of looking for multiple sources of scattering that depend on frequency. Having that in mind, the large frequency bandwidth is crucial for decreasing the number of minima in the solution space where the metric $F$ (Eq. (6) is minimized, and therefore for efficiently discriminating between scattering sources with very different sizes.

The results of this wide band study provide a better understanding of the ranges in which the QUS parameter values lie. In particular, the QUS parameter estimates suggest that the dominant sources of scattering are the whole hepatocytes. Several previous studies have already compared

ESD values, obtained with various BSC models, to histological observations[26,35,37]. As opposed to the present work, these experiments were performed on narrower frequency bands. Furthermore, the use of models such as SGM or FSM, which do not take into account packing effects due to density or polydispersity, lead to conclusions that need to be mitigated[26,35,37]. On the contrary, ESD close to HMD were reported when using poly-SFM[38].

The frequency range of used in this study [10-52] MHz is large to estimate microstructural parameters at the scale of the nuclei or whole cells but also to enable real-time monitoring of non-invasive HIFU procedures in *in vivo* at the lowest frequencies values. Central frequencies of abdominal imaging probes generally lie between 4 and 7 MHz. However, higher frequencies (10 to 15 MHz) are commonly used in the case of more superficial scanning or for intraoperative applications. Indeed, ultrasound-guided intraoperative treatments using HIFU, radiofrequency, laser or micro-waves have been widely developed for the past several years[39,40,41] and references therein). Our results are thus relevant with various *in vivo* applications which will be further investigated in future work.

Furthermore, this research provides valuable information regarding the underlying physical phenomena that occur during the heating process and remain thereafter . This information could be used as *a priori* knowledge at lower frequencies for the estimation of QUS parameters. Indeed, once the whole hepatocytes are hypothesized to be responsible for scattering, one could envision weighing frequencies in the cost functions according to the expected resonance peaks in the BSC, or or imposing greater constraints on the bounds of QUS parameters during the optimization procedure. Further studies need to be conducted at lower frequencies to evaluate these new inversion strategies on the basis of this *a priori* knowledge.

# V. Conclusion

The results presented in this study provide a description of the impact of thermal ablation in human liver tissue on acoustic attenuation and the BSC. BSCs were measured in the frequency range from 10 to 52 MHz, and the polydisperse structure factor model was used to extract structural parameters, with a particular focus on the Effective Scatterer Diameter (ESD). The attenuation was measured to twice the value after thermal ablation at temperatures above 70°C as compared to

its value before ablation. Regarding the BSC, an average increase by a factor of 4 is observed after ablation at the maximum temperature of 80°C.

ESDs before and after heating were compared to histological observations, with the objective of determining the nature of the principal source of scattering in human liver tissue. For the first time, quantitative agreement between the ESD and hepatocyte mean diameter (HMD) was shown for both unheated and heated samples at temperatures comparable to those reached during thermal ablation. This result reveals the predominant role of cells in scattering, compared to other structures such as nuclei.

If our experiments were carried in a frequency range inaccessible to non-invasive clinical probes, they could be useable in an intraoperative context. Indeed, the physical understanding of BSC behavior after thermal ablation at high frequencies can be of great interest for imposing constraints on the bounds of QUS parameters during the optimization procedure on a narrower frequency window. Therefore, our work paves the way for using QUS methods to monitor structural changes during thermal ablation.

# Declarations

This work was partly funded by France Life Imaging (grant ANR-11-INBS-0006) and the French National Research Agency (ANR-19-CE19-0027-01).

# Appendices

## A $\text{BSC}_{\text{poly-SFM}}$ variations with different QUS parameters

Relation between $\text{BSC}_{\text{poly-SFM}}$ and ESD, concentration $\phi$ and gamma width factor $\zeta$ are not trivial (see Eq. (3)). As a result, evolutions of $\text{BSC}_{\text{poly-SFM}}$ with respect to each of these parameters are reported in Figures A(1), (2) and (3).

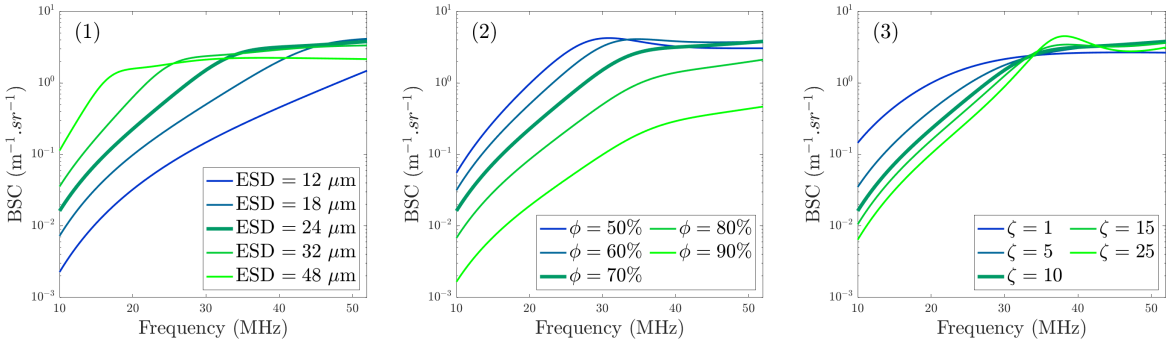


Figure A: $\text{BSC}_{\text{poly-SFM}}$ estimated for different values of (1) ESD, (2) concentration $\phi$ and (3) gamma width factor $\zeta$. The thick line is common to the three figures and is obtained with ESD $= 24$ $\mu$m, $\zeta = 10$, $\phi = 70\%$ and $\gamma = 0.05$.

## B Estimation of concentration $\phi$ and impedance contrast $\gamma_z$ for before and after thermal exposure.

The two QUS parameters concentration $\phi$ and impedance contrast $\gamma_z$ are shown in Figure B(1) and (2), for the same five samples that were histologically analyzed in section IV.

Figure B(1) reveals that the impedance contrast $\gamma_z$ remained low after the heating process and was almost unchanged for the two samples heated up to temperature $T \leq 55°\text{C}$. At the highest temperature $T = 80°\text{C}$ it reached its maximum value $\gamma_z = 0.082$. Note that estimates of $\gamma_z$ never reach the upper bound value of 0.1 (refer to Table 1). This indicates the existence of a local minimum in the interval [0.01-0.1], which corresponds to a physically acceptable solution considering the assumption of scattering by fluid particles.

The spatial concentration $\phi$ is shown in Fig. B(2). For this quantity, only the nonphysical solution $\phi > 1$ was excluded from the interval considered in the optimization process (Table 1). The most significant effect is observed at $T = 80°\text{C}$. For this temperature, a decrease of 37% is

predicted by poly-SFM.

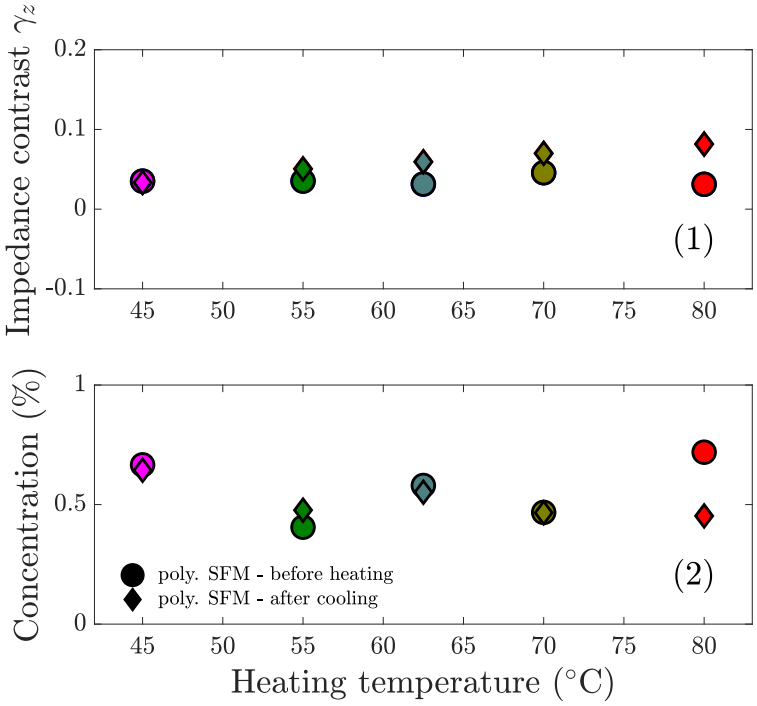


Figure B: (1) Impedance contrast $\gamma_z$ and (2) concentration $\phi$ for the five samples shown in Figure 6, before heating (circles) and after cooling (diamonds).


[1] N. T. Sanghvi, W.-H. Chen, R. Carlson, C. Weis, R. Seip, T. Uchida, and M. Marberger, Clinical validation of real-time tissue change monitoring during prostate tissue ablation with high intensity focused ultrasound, Journal of Therapeutic Ultrasound **5**, 24 (2017).

[2] K. Yang, Q. Li, H.-L. Liu, C.-K. Chen, C.-W. Huang, J.-R. Chen, Y.-W. Tsai, Z. Zhou, and P.-H. Tsui, Frequency-domain CBE imaging for ultrasound localization of the HIFU focal spot: a feasibility study, Scientific Reports **10**, 5468 (2020).

[3] X. Li, G. Ghoshal, R. J. Lavarello, and M. L. Oelze, Exploring potential mechanisms responsible for observed changes of ultrasonic backscattered energy with temperature variations: Changes in ultrasonic backscattered energy with temperature, Medical Physics **41**, 052901 (2014).

[4] M. L. Oelze and W. D. O'Brien, Application of Three Scattering Models to Characterization of Solid Tumors in Mice, Ultrasonic Imaging **28**, 83–96 (2006).

[5] G. Ghoshal, J. P. Kemmerer, C. Karunakaran, R. J. Miller, and M. L. Oelze, Quantitative Ultrasound for Monitoring High-Intensity Focused Ultrasound Treatment In Vivo, IEEE Transactions on Ultrasonics, Ferroelectrics, and Frequency Control **63**, 1234–1242 (2016).

[6] K. J. Parker, Shapes and distributions of soft tissue scatterers, Physics in Medicine & Biology **64**, 175022 (2019).

[7] K. A. Wear, Frequency dependence of ultrasonic backscatter from human trabecular bone: Theory and experiment, The Journal of the Acoustical Society of America **106**, 3659–3664 (1999).

[8] G. Ferraioli and L. B. S. Monteiro, Ultrasound-based techniques for the diagnosis of liver steatosis, World Journal of Gastroenterology **25**, 6053–6062 (2019).

[9] D. T. Fetzer, I. M. Rosado-Mendez, M. Wang, M. L. Robbin, A. Ozturk, K. A. Wear, J. Ormachea, T. A. Stiles, J. B. Fowlkes, T. J. Hall, and A. E. Samir, Pulse-Echo Quantitative US Biomarkers for Liver Steatosis: Toward Technical Standardization, Radiology **305**, 265–276 (2022).

[10] Z. F. Lu, J. Zagzebski, and F. Lee, Ultrasound backscatter and attenuation in human liver with diffuse disease, Ultrasound in Medicine & Biology **25**, 1047–1054 (1999).

[11] F. Lizzi, M. Ostromogilsky, E. Feleppa, M. Rorke, and M. Yaremko, Relationship of Ultrasonic Spectral Parameters to Features of Tissue Microstructure, IEEE Transactions on Ultrasonics, Ferroelectrics and Frequency Control **34**, 319–329 (1987).

[12] M. Insana, R. Wagner, D. Brown, and T. Hall, Describing small-scale structure in random media using pulse-echo ultrasound, J Acoust Soc Am. **87**, 179–92 (1990).

[13] R. De Monchy, J. Rouyer, F. Destrempes, B. Chayer, G. Cloutier, and E. Franceschini, Estimation of polydispersity in aggregating red blood cells by quantitative ultrasound backscatter analysis, The Journal of the Acoustical Society of America **143**, 2207–2216 (2018).

[14] V. Suomi, Y. Han, E. Konofagou, and R. O. Cleveland, The effect of temperature dependent tissue parameters on acoustic radiation force induced displacements, Physics in Medicine and Biology **61**, 7427–7447 (2016).

[15] Y. Takahashi, Histopathology of nonalcoholic fatty liver disease/nonalcoholic steatohepatitis, World Journal of Gastroenterology **20**, 15539 (2014).

[16] J. Timaná, H. Chahuara, L. Basavarajappa, A. Basarab, K. Hoyt, and R. Lavarello, Simultaneous imaging of ultrasonic relative backscatter and attenuation coefficients for quantitative liver steatosis assessment, Scientific Reports **13**, 8898 (2023).

[17] J. Mamou and M. L. Oelze, Quantitative Ultrasound in Soft Tissues, volume 1, Springer Dordrecht, 2013.

[18] M. Sanchez, V. Barrere, I. Treilleux, N. Chopin, and D. Melodelima, Development of a noninvasive HIFU treatment for breast adenocarcinomas using a toroidal transducer based on preliminary attenuation measurements, Ultrasonics **115**, 106459 (2021).

[19] L. X. Yao, J. A. Zagzebski, and E. L. Madsen, Backscatter coefficient measurements using a reference phantom to extract depth-dependent instrumentation factors, Ultrasonic imaging **12**, 58–70 (1990).

[20] E. L. Madsen, F. Dong, G. R. Frank, B. S. Garra, K. A. Wear, T. Wilson, J. A. Zagzebski, H. L. Miller, K. K. Shung, S. H. Wang, E. J. Feleppa, T. Liu, W. D. O'Brien, K. A. Topp, N. T. Sanghvi, A. V. Zaitsev, T. J. Hall, J. B. Fowlkes, O. D. Kripfgans, and J. G. Miller, Interlaboratory comparison of ultrasonic backscatter, attenuation, and speed measurements., Journal of Ultrasound in Medicine **18**, 615–631 (1999).

[21] X. Chen, D. Phillips, K. Q. Schwarz, J. G. Mottley, and P. K. J, The measurement of backscatter coefficient from a broadband pulse-echo system: a new formulation, IEEE Transactions on Ultrasonics, Ferroelectrics, and Frequency Control **44**, 512–525 (1997).

[22] V. C. Anderson, Sound Scattering from a Fluid Sphere, The Journal of the Acoustical Society of America **22**, 426–431 (1950).

[23] E. Franceschini, R. d. Monchy, and J. Mamou, Quantitative Characterization of Tissue Microstructure in Concentrated Cell Pellet Biophantoms Based on the Structure Factor Model, IEEE Transactions on Ultrasonics, Ferroelectrics, and Frequency Control **63**, 1321–1334 (2016).

[24] A. Han and W. D. O'brien, Structure function for high-concentration biophantoms of polydisperse scatterer sizes, IEEE Transactions on Ultrasonics, Ferroelectrics, and Frequency Control **62**, 303–318 (2015).

[25] W. L. Griffith, R. Triolo, and A. L. Compere, Analytical scattering function of a polydisperse Percus-Yevick fluid with Schulz- ($\Gamma$-) distributed diameters, Phys. Rev. A **35**, 2200–2206 (1987).

[26] J. P. Kemmerer and M. L. Oelze, Ultrasonic Assessment of Thermal Therapy in Rat Liver, Ultrasound in Medicine & Biology **38**, 2130–2137 (2012).

[27] N. Maklad, J. Ophir, and V. Balsara, Attenuation of ultrasound in normal liver and diffuse liver disease in vivo, Ultrasonic Imaging **6**, 117–125 (1984).

[28] N. A. Manaf, D. S. Ridzuan, M. I. M. Salim, and K. W. Lai, Measurement of Ultrasound Attenuation and Protein Denaturation Behavior During Hyperthermia Monitoring, pages 205–222, Springer Singapore, Singapore, 2015.

[29] K. P. Mercado, M. Helguera, D. C. Hocking, and D. Dalecki, Estimating Cell Concentration in Three-Dimensional Engineered Tissues Using High Frequency Quantitative Ultrasound, Annals of Biomedical Engineering **42**, 1292–1304 (2014).

[30] C. Segnani, C. Ippolito, L. Antonioli, C. Pellegrini, C. Blandizzi, A. Dolfi, and N. Bernardini, Histochemical Detection of Collagen Fibers by Sirius Red/Fast Green Is More Sensitive than van Gieson or Sirius Red Alone in Normal and Inflamed Rat Colon, PLOS ONE **10**, e0144630 (2015).

[31] K. Tamura, J. Mamou, K. Yoshida, T. Yamaguchi, and E. Franceschini, Quantifying scattering from dense media using two-dimensional impedance maps, The Journal of the Acoustical Society of America **148**, 1681–1691 (2020).

[32] M. Roncalli, M. Borzio, M. V. Tombesi, A. Ferrari, and E. Servida, A morphometric study of liver cell dysplasia, Human Pathology **19**, 471–474 (1988).

[33] E. Franceschini, R. Guillermin, F. Tourniaire, S. Roffino, E. Lamy, and J.-F. Landrier, Structure factor model for understanding the measured backscatter coefficients from concentrated

cell pellet biophantoms, The Journal of the Acoustical Society of America **135**, 3620–3631 (2014).

[34] O. Falou, M. Rui, A. El Kaffas, J. C. Kumaradas, and M. C. Kolios, The measurement of ultrasound scattering from individual micron-sized objects and its application in single cell scattering, The Journal of the Acoustical Society of America **128**, 894–902 (2010).

[35] P. Muleki-Seya, R. Guillermin, J. Guglielmi, J. Chen, T. Pourcher, E. Konofagou, and E. Franceschini, High-Frequency Quantitative Ultrasound Spectroscopy of Excised Canine Livers and Mouse Tumors Using the Structure Factor Model, IEEE Transactions on Ultrasonics, Ferroelectrics, and Frequency Control **63**, 1335–1350 (2016).

[36] F. Insana and J. Hall, Ultrasound imaging from backscatter measurements: image formation and interpretation, Ultrason. Imag. **12**, 245–267 (1990).

[37] A. D. Pawlicki, A. J. Dapore, S. Sarwate, and W. D. O'Brien, Three-dimensional impedance map analysis of rabbit liver, The Journal of the Acoustical Society of America **130**, EL334–EL338 (2011).

[38] E. Franceschini, J.-M. Escoffre, A. Novell, L. Auboire, V. Mendes, Y. M. Benane, A. Bouakaz, and O. Basset, Quantitative Ultrasound in Ex Vivo Fibrotic Rabbit Livers, Ultrasound in Medicine & Biology **45**, 1777–1786 (2019).

[39] D. Melodelima, W. A. N'Djin, J. Favre-Cabrera, H. Parmentier, M. Rivoire, and J. Y. Chapelon, Thermal ablation produced using a surgical toroidal high-intensity focused ultrasound device is independent from hepatic inflow occlusion, Physics in Medicine Biology **54**, 6353 (2009).

[40] T. Yang, D. M. Ng, N. Du, N. He, X. Dai, P. Chen, F. Wu, B. Chen, X. Fan, K. Yan, X. Zhou, M. Dong, Z. Zheng, and L. Gu, HIFU for the treatment of difficult colorectal liver metastases with unsuitable indications for resection and radiofrequency ablation: a phase I clinical trial, Surgical Endoscopy **35**, 2306–2315 (2021).

[41] A. Dupré, M. Rivoire, S. Metzger, C. Cropet, J. Vincenot, P. Peyrat, Y. Chen, D. Pérol, and D. Melodelima, Intra-operative High-Intensity Focused Ultrasound in Patients With Colorectal Liver Metastases: A Prospective Ablate-and-Resect Study, Ultrasound in Medicine Biology **49**, 1845–1851 (2023).